A perfectly inelastic collision: Bulk prey engulfment by baleen whales and dynamical implications for the world's largest cetaceans

Jean Potvin, David E. Cade, Alexander J. Werth, Robert E. Shadwick, and Jeremy A. Goldbogen

Citation: American Journal of Physics **88**, 851 (2020); doi: 10.1119/10.0001771
View online: https://doi.org/10.1119/10.0001771
View Table of Contents: https://aapt.scitation.org/toc/ajp/88/10
Published by the American Association of Physics Teachers

A perfectly inelastic collision: Bulk prey engulfment by baleen whales and dynamical implications for the world's largest cetaceans

Jean Potvin
Department of Physics, Saint Louis University, St. Louis, Missouri 63103

David E. Cade[a)]
Hopkins Marine Station, Stanford University, Pacific Grove, California 93950

Alexander J. Werth
Department of Biology, Hampden-Sydney College, Hampden-Sydney, Virginia 23943

Robert E. Shadwick
Department of Zoology, University of British Columbia, Vancouver, British Columbia, Canada V6T 1Z4

Jeremy A. Goldbogen
Hopkins Marine Station, Stanford University, Pacific Grove, California 93950

(Received 12 February 2020; accepted 15 July 2020)

The largest animals are the rorquals, a group of whales which rapidly engulf large aggregations of small-bodied animals along with the water in which they are embedded, with the latter subsequently expulsed via filtration through baleen. Represented by species like the blue, fin, and humpback whales, rorquals can exist in a wide range of body lengths (8–30 m) and masses (4000–190,000 kg). When feeding on krill, kinematic data collected by whale-borne biologging sensors suggest that they first oscillate their flukes several times to accelerate towards their prey, followed by a coasting period with mouth agape as the prey-water mixture is engulfed in a process approximating a perfectly inelastic collision. These kinematic data, used along with momentum conservation and time-averages of a whale's equation of motion, show the largest rorquals as generating significant body forces (10–40 kN) in order to set into forward motion enough engulfed water to at least double overall mass. Interestingly, a scaling analysis of these equations suggests significant reductions in the amount of body force generated per kilogram of body mass at the larger sizes. In other words, and in concert with the allometric growth of the buccal cavity, gigantism would involve smaller fractions of muscle mass to engulf greater volumes of water and prey, thereby imparting a greater efficiency to this unique feeding strategy.
https://doi.org/10.1119/10.0001771

I. INTRODUCTION

In the mechanics of living systems, movement and dynamics end up tightly coupled to body physiology and morphology, as animals use muscle to perform the work to swim and collect prey.[1] Such couplings are spectacularly exemplified by the rorqual whales (Mysticeti: Balaenopteridae), a subgroup of large cetaceans measuring 8–30 m in length and 4000–190,000 kg in mass (Fig. 1).[2–5] Rorquals, which include the blue whale (*Balaenoptera musculus*), fin whale (*Balaenoptera physalus*), and humpback whale *(Megaptera novaeangliae)* (Fig. 1), are edentulous filter-feeders that forage on aggregations of small prey, typically patches of plankton (krill) or schools of small forage fish (anchovies, capelin, and the like).[2,4,5] To do this, rorquals have evolved morphologies and adopted a unique prey-acquisition strategy—lunge feeding—which enhances bulk prey collection (Fig. 2). As shown here, the manners in which lunge feeding is carried out, i.e., in terms of foraging durations and swim speeds at the moment of prey capture, become a crucial element for not only determining how much force need be applied, but also for constraining how evolution or growth to large body size might have been suppressed or favored.[4]

Rorquals feed by first approaching a large aggregation of prey at high fluking frequency to build up speed. This is followed by the whales engulfing both prey and the water in which it is embedded, with the latter being subsequently expulsed out of the then-inflated buccal cavity via through-baleen filtration (Fig. 2).[3,6] The rorquals' success in capturing enough food to meet the energetic demands of their large body not only depends on prey availability,[7] but also on their capacity to swim fast enough to defeat the escape strategies of the prey[8] and, as discussed below, to generate the requisite body forces to engulf and set into forward motion extreme amounts of prey-laden water, namely, up to 240,000 kg at the largest size (Fig. 2).[2,9–11] Such forces are the fluking thrust generated by the tail musculature, and the forward push onto the engulfed mass via tension of the muscle embedded in the Ventral Groove Blubber (VGB) (Fig. 2).[10–15]

Rorquals have been observed lunge feeding in multiple ways: Individually or in groups, while lunging along the surface or at depth and generally along an uphill track (Fig. 2); or collectively again, but doing so vertically while breaking the surface after enclosing the prey within a "net" of bubbles.[16] A distinction is made here between lunges in which the engulfment stage is carried out (Figs. 2 and 3), that is, while fluking ("powered engulfment") or coasting ("coasting engulfment"). Powered engulfment has been observed mostly against schooling fish near the surface

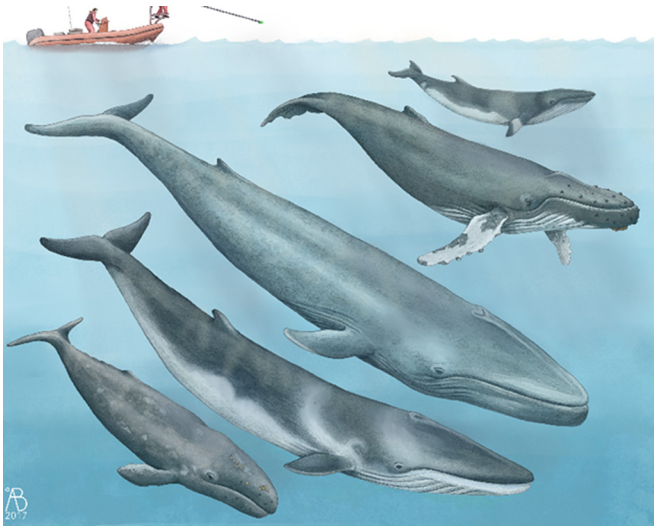

Fig. 1. A family portrait of giants, drawn in proportion to biologists deploying archival trajectory sensors (or "tags"). From top to bottom: minke, humpback, blue, and fin members of the rorqual family; also shown along with another baleen whale, the grey whale (*Eschrichtius robustus*), a bottom-feeder. Artwork by Alex Boersma; reproduced with permission.

where the escape paths are spatially limited, often by the presence of multiple predators[17,18] or by curtains of bubbles blown around fish to encourage aggregation.[16,19] On the other hand, drone video and accelerometer sensors deployed on krill-feeding whales suggest rorquals coasting during most of the engulfment stage, i.e., after carrying out one or two low-frequency fluking strokes as the mouth opens.[2]

Coasting engulfment is a process analogous to the perfectly inelastic collision of (similar) Velcroed balls studied in introductory physics experiments. Neglecting frictional drag, this is an interaction in which the total momentum of the body and engulfed water is conserved, and also one in which a significant portion of the momentum gained by the whale during prey approach is lost to the prey-water mixture being engulfed. Building-up total momentum prior to *and* during engulfment has been proposed before,[20] but in powered engulfment scenarios in which the momentum gained is used to reduce fluking intensity in the later stages of engulfment. In the context of the engulfing prey while coasting, a high prey-approach momentum build-up is required to generate the requisite decelerative motion that is to last throughout the duration of engulfment. This is a requirement for a high-speed approach, but one which carries a smaller overhead in drag as discussed here.

Coasting engulfment occurs either at depth or at the surface and is carried out by most rorqual species, particularly when feeding on krill. Such a feeding mode is also used by the blue whale—the largest marine vertebrate and an obligate krill feeder—and therefore presents a useful case study of the impact of physics on the kinematics and dynamics of large body size. A recent study of the feeding energy efficiency by baleen whales foraging on plankton aggregations (including krill) has shown high captured prey energy per units of (predator) metabolic energy expended, in comparison to single-prey item foraging by smaller toothed whales.[7]

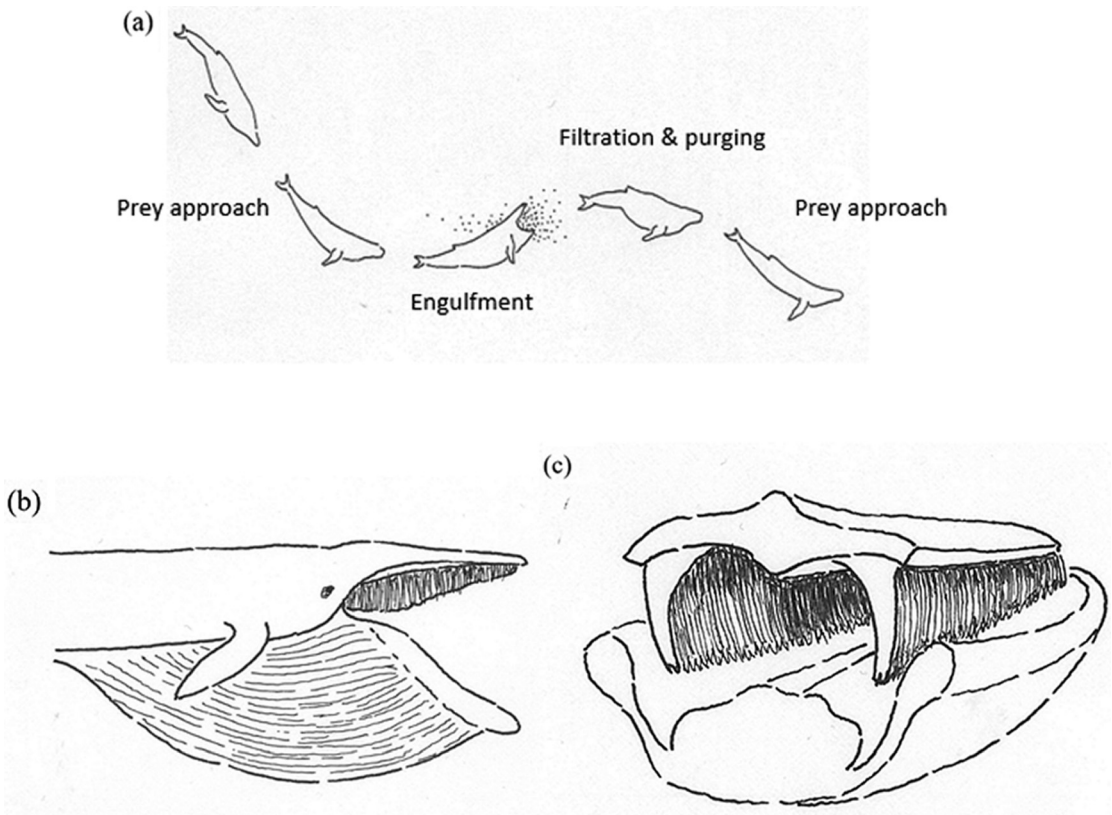

Fig. 2. (a) The stages of lunge-feeding—prey-approach, engulfment, and water expelling via filtration, which may be repeated in successive lunges through the same patch of prey. (b) Profile of the inflated buccal cavity during engulfment showing the distended ventral skin, also known as the Ventral Groove Blubber (VGB) (Refs. 12–15); and (c) a cut-out view of the baleen plates hanging from the palatal gingiva, in relation to the tongue and ventral section of the mouth. Diagrams adapted by Deborah Albert with permission from A. Boersma (top) and Center for Coastal Studies, Provincetown, MA (bottom).

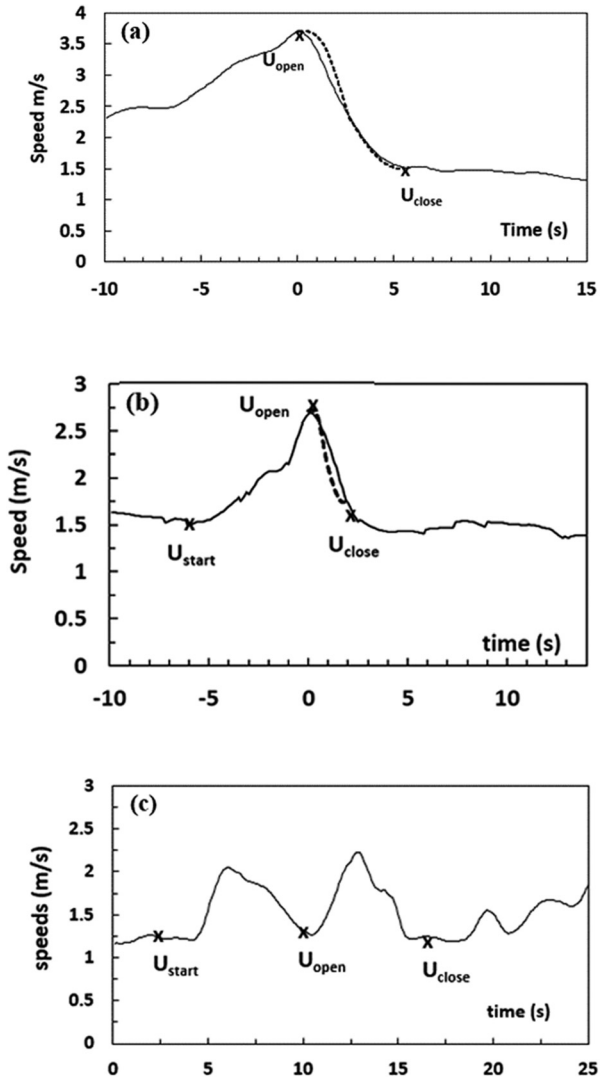

Fig. 3. Speed profiles of lunge-feeding rorquals obtained from tag data (continuous lines) (Ref. 17). Examples of 22 m blue (a) and 8 m humpback (b) whales accelerating towards their prey (krill), and then engulfing without fluking, a purely decelerative stage. The dashed lines show results of simulations of the engulfment stage using a time-dependent hydrodynamic model (Ref. 11). (c) The case of a 10 m humpback whale fluking while engulfing fish. U_{start}, U_{open}, and U_{close} correspond to the swim speeds at the beginning of prey approach, mouth opening, and mouth closing, respectively. In all three cases, body size was reconstructed from allometric relationships of body length to the length of the ventral throat pouch as determined by speed and timing of engulfment events (Ref. 17).

A different question is to be explored here, namely, the connection between dynamics, as represented by propulsion and engulfment forces (rather than energy), morphology (body mass and inflated buccal cavity volume[21,22]), and kinematics (prey approach and engulfment duration and speed); and ultimately, whether this connection scales at large body size to favor gigantism regardless of prey abundance. This shall be established by considering a time-averaged version of the equations of motion for a whale and its engulfed mass, as informed by the swim speeds (at mouth opening) and engulfment durations obtained from bio-logging tags deployed on dozens of free ranging whales (Figs. 1, 4, and 5).[17] Such tags are equipped with accelerometers, gyroscopes, magnetometers, hydrophones, pressure sensors, and cameras, to document behaviors which, for the most part, have remained out

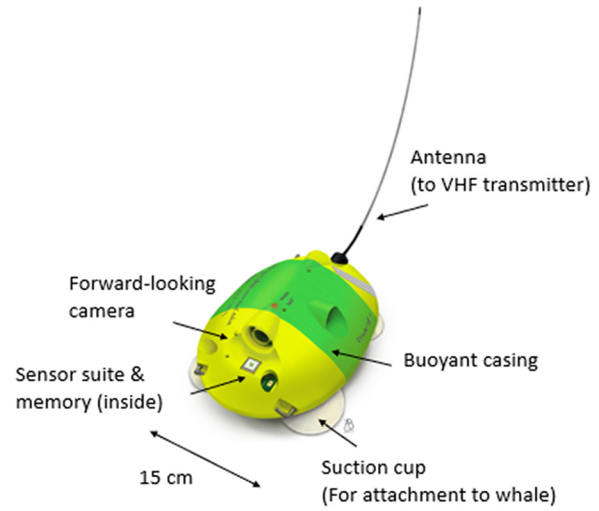

Fig. 4. Typical bio-logging tag used for tracking whale behavior and feeding kinematics.

of view (Fig. 5).[23] The kinematic data thus obtained will be described in Sec. III, following the presentation in Sec. II of general time-averaged force equations for krill-feeding lunges. Section III will also present a new non-dimensional description of engulfment durations used in body-size scaling. Section IV presents new results on engulfment forces,

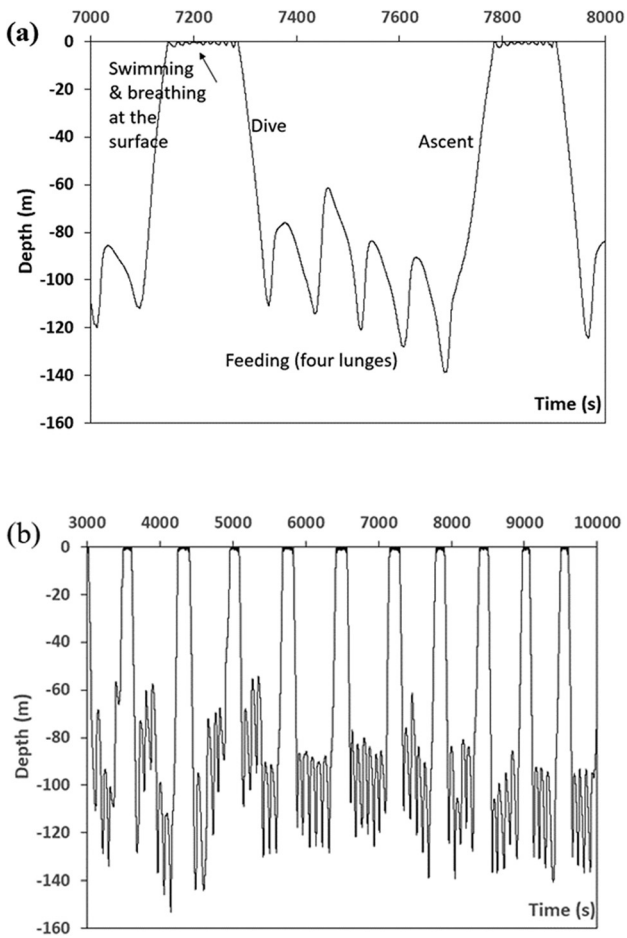

Fig. 5. Tag-recorded swim depth versus time, over an 8-hour feeding bout on krill by a 27 m blue whale (tag bw160727-10). Short (a), versus longer series (b) from the same bout (Ref. 17).

here seen as mediating the (approximated) perfect inelastic collision between a whale and its engulfed mass. These results are used in Sec. V in a scaling study of engulfment capacity and force with respect to body size. Derivations of several new equations are found in Appendices A–D which follow the Concluding Remarks in Sec. VI.

II. MATERIALS AND METHODS—THE FORCES AT PLAY

The schematics of the forces acting on a whale and the (to be) engulfed mass are shown in Fig. 6. Here, body weight (W) and buoyancy (B) turn out to be unimportant as they nearly cancel each other out, at least near the surface where buoyancy is controlled by lung volume expansion and depression via breathing.[24] At depths below 60–100 m, compression of the thorax makes the body negatively buoyant ($B < W$), an imbalance likely compensated for by the lift generated by the tilting of the foil-shaped flippers[25,26] and head[27] (in similarity with sharks[28]).

More important is the fluking thrust and body drag generated in both mouth-open and -closed configurations. As "thunniform" swimmers, whales are hydrodynamically simpler than (undulating) fishes, with thrust production limited to the rear end of the body (the flukes) and drag generation to the rest (including the caudal tail).[29,30] To this picture, and during engulfment, one adds the so-called "engulfment drag" ($F_D{}^{engulf}$) generated in reaction to the forward push onto the engulfed mass by VGB musculature,[15] and "shape drag" ($F_D{}^{shape}$), which is connected to the friction and longitudinal pressure gradient generated by the flows moving externally to the body[10,11]—a force herein shown to be comparatively small (Sec. IV).

Assuming one-dimensional kinematics and during prey approach, a whale's equation of motion is given by $M_{body}\, a_{whale} = Thrust$, and during engulfment by $M_{body}\, a_{whale} = Thrust - F_D{}^{engulf}$ (powered) or $M_{body}\, a_{whale} = -F_D{}^{engulf}$ (coasting). Another equation will account for prey-water mixture motion via $d(M_{water}\, U_{water})/dt = +F_D{}^{engulf}$. In contrast to coasting engulfment, the total momentum of the whale-mixture system during powered engulfment isn't conserved due to the non-zero impulse by fluking thrust. Moreover, and in both engulfment cases, the system's total kinetic energy isn't conserved either, due to the contribution of the fluking tail (powered engulfment), and the energy spent by the VGB forces (musculature[10–12] and/or elastic[20]) to control ventral cavity expansion (both scenarios) (Figs. 1 and 2). Such an expansion is a "deformation" of the whale body both orthogonally and along the direction of motion, and accounts for the extra work spent by the whale-mixture contact forces in work-energy treatments of perfectly inelastic collisions.[31]

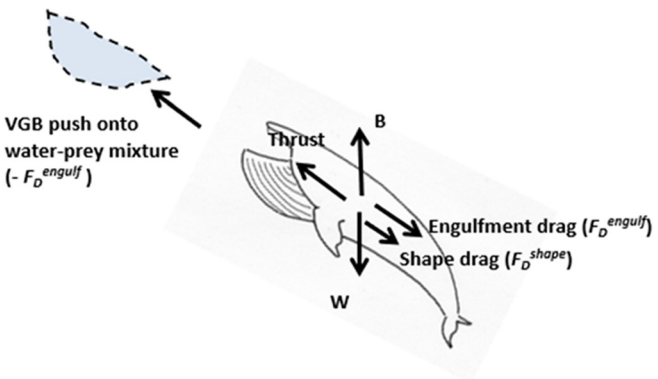

Fig. 6. Forces on a lunge-feeding whale and its engulfed mass (shaded) (Ref. 10). Symbol *B* corresponds to buoyancy, or to buoyancy plus lift when the latter is needed to help counteract the weight (*W*).

Between drag and thrust, the former is generally the better-known force and more amenable to formulation in an equation. In a previous study,[11] time-dependent engulfment forces were expressed in parametric form based on assumed rates of the mouth opening and best-fit parameters (Fig. 3). A simpler, yet more general alternative is used here. Writing down a mathematical expression for the total drag is complicated by the fact that the drag itself is a reaction to the "active" forces of the fluking tail and VGB, i.e., as driven by muscle contractions informed by auditory, visual, and other sensory cues.[32] But time-averaged values of the Newtonian equation of motion can be derived regardless of muscle contraction specifics. In reference to Figs. 3 and 6, and assuming straight-line trajectories, one has the following in the case of prey approach (a closed-mouth state):

$$\left\langle F_{thrust} - F_{drag}{}^{shape} \right\rangle = \left\langle \frac{d}{dt}\left(M_{body} U(t)\right) \right\rangle = \frac{M_{body}(U_{open} - U_{start})}{T_{approach}}, \tag{1}$$

and during coasting engulfment (an open-mouth state),[33]

$$\left\langle F_{drag}{}^{engulf} + F_{drag}{}^{shape} \right\rangle = -\left\langle \frac{d}{dt}\left(M_{body} U(t)\right) \right\rangle = \frac{M_{body}(U_{open} - U_{close})}{T_{\text{engulf}}}. \tag{2}$$

Such results aren't very useful where the laws of force are known *a priori*—as in most introductory college physics examples. But in cases of active, muscle-driven forces with temporal variations likely to differ from lunge to lunge and even from individual to individual, Eqs. (1) and (2) become relevant, if not fundamental, for being independent of any force-vs-time profiles of same-duration, initial velocity, and final velocity.

Equations (1) and (2) use tag-derived inputs, namely, parameters U_{open}, U_{close}, and T_{engulf} corresponding to the forward speeds at mouth opening and at closure times, and to engulfment duration, respectively; and U_{start} and $T_{approach}$, to a whale's speed at the beginning of prey approach, and prey approach duration, respectively (Fig. 3). Here, one assumes $U_{start} \approx U_{close}$, as suggested by the data of Fig. 3 (middle frame) and other tag data.[17] Equation (2) informed by the data in Fig. 3 suggests a net force of about 40 kN when generated by a 100,000 kg blue whale engulfing prey and water with speed decrements of $\approx$2m/s over $\approx$5s duration. On the other hand, the average thrust can be estimated from Eq. (1) and the data of Table I, i.e., after calculating the average closed mouth body drag from the approximation described in Appendix A. The manners in which Eqs. (1) and (2) increase with body size will rest with the size-scaling of the durations and speeds discussed in Secs. III and V.

III. RESULTS—SPEEDS AND DURATIONS

A. Tag-measured speeds and durations

Bio-logging tags have provided a unique look at krill-feeding at depth (Fig. 5),[17] with examples of forward speeds

Table I. Morphological and physical characteristics. Body length and swim speed at mouth opening were measured and all other parameters estimated from the indicated references. Asterisks mark averages over values recorded over all lunges detected by the bio-logging tag (Ref. 17). Standard deviations (SD) were obtained from analysis of the tag data (Ref. 17) and a morphology database (Ref. 21).

	Humpback whale	Blue whale	Blue whale	Remarks
M_{body} (kg) (SD)	8000 (8000)	67,273 (23,991)	129,005 (46,081)	Ref. 21 (blue whale); and Ref. 11 (humpback whale). SD for both species from Ref. 11
L (m) Bio-logging Tag Number	8 mn 160727-11	22.72 bw160224-8	27.40 bw160727-10	Ref. 17
Number of lunges from Tag sampling	34	4	17	…
L_{VGB} (m) (SD)	4.31 (0.21)	12.99 (0.26)	16.36 (0.32)	Ref. 21.
L_{jaw} (m) (SD)	1.62 (0.13)	4.34 (0.31)	5.65 (0.41)	Ref. 21
W_{head} (m) (SD)	1.32 (0.16)	2.61 (0.15)	3.27 (0.19)	Ref. 21
S_{wet} (m^2)	27.5	109.9	167.9	Refs. 29 and 36
U_{open} (m/s) (averaged) (SD)	3.56 (0.26)	2.78 (0.13)	3.25 (0.33)	Ref. 17 and Fig. 7
M_{water} (kg) (SD)	4,982 (290)	90,350 (1,648)	185,595 (3,446)	Eq. (5); SD from Ref. 21.
M_{water} /M_{body} (SD)	0.67 (0.32)	1.33 (0.02)	1.40 (0.03)	Ref. 17
U_{close} (m/s) (SD)	2.19 (0.55)	1.19 (0.15)	1.33 (0.36)	Eq. (4)
Engulfment time T_{engulf} (s) * (SD)	1.18 (0.16)	5.65 (0.45)	6.58 (0.76)	Ref. 17 and Fig. 7
Prey-approach time (s) * (SD)	16.5 (8.9)	13.5 (3.9)	19.519.5 (10.0)	Ref. 17 and Fig. 7
Purging time (s) *	27.5 (3.7)	61.9 (12.2)	48.8 (9.6)	Ref. 17 and Fig. 7
U_{open}/T_{engulf} (m/s^2) (SD)	3.07 (0.49)	0.50 (0.04)	0.52 (0.07)	Ref. 17
U_{open}/$T_{approach}$ (m/s^2) (SD)	0.27 (0.11)	0.22 (0.06)	0.20 (0.08)	Ref. 17
$\langle F_{thrust} + F_D^{shape} \rangle$ (N)	664 (796)	7,922 (4,673)	12,702 (9,272)	$U_{start} \approx\sim U_{close}$ Eq. (1); Refs. 17 and 21 for kinematics and morphology
$\langle F_D^{engulf} \rangle$ (N) (SD)	9,262 (2,271)	18,973 (3,704)	37,590 (13,420)	Eq. (6); Refs. 17 and 21 for kinematics and morphology
$\langle F_D^{engulf} \rangle$/$M_{body}$ (m/s^2) (SD)	1.15 (0.74)	0.28 (0.03)	0.29 (0.04)	Eq. (6); Refs. 17 and 21 for kinematics and morphology
$\langle F_D^{engulf} + F_D^{shape} \rangle$ (N) (SD)	9,288 (10,867)	18,931 (7,951)	37,642 (18,068)	Eq. (2); Refs. 17 and 21 for kinematics and morphology
$F_D^{engulf}\|_{max}$ (N) (SD)	24,732 (6,183)	50,568 (10,114)	100,365 (35,127)	Eq. (7); Refs. 17 and 21 for kinematics and morphology

at the moment of mouth opening (U_{open}) and durations of both prey approach and engulfment shown in Figs. 3 and 7. Speeds are determined from exponential relationships of flow noise and accelerometer vibrations,[34] from video-based feeding duration (when available), and from accelerometer signals indicating fluking on approach (U_{start}) as well as deceleration during engulfment (U_{open} to U_{close}).[17,18] Interestingly, Fig. 7 shows a surprising degree of kinematic regularity on a lunge-to-lunge and dive-to-dives basis. Also noticeable are the systematic variations among similarly sized blue whales which aren't well understood. Such regularity is likely enabled by slow-moving krill (≈0.1–0.2 m/s)[35] living in aggregations that considerably exceed a whale's body size, thereby presenting an essentially immobile target[18] when approached at speeds exceeding 2.5–5.0 m/s (top frame). At 6 s on average, engulfment is the shorter of the three stages of lunge feeding (Fig. 7), i.e., versus the 15–20 s during prey approach and the 50–100 s during purging and filtration. The reasons for these different durations are not very well understood, but are likely to depend on the temporal changes of the prey patch's shape and mass density, and occur, e.g., when a whale repeatedly lunges through the same patch during the same feeding dive (Fig. 5).

B. Non-dimensional formulation

The scatter in U_{open} and T_{engulf} (Fig. 7), coupled with relatively small sample sizes currently prevents robust empirical determinations of the relationship between those observables. On the other hand, viewing an engulfing whale as an inflating bag or parachute suggests the idea that, for the same (time-averaged) inlet area, a faster whale engulfs/inflates more rapidly than a slower one. This follows from the conservation of the fluid mass accumulating in the buccal cavity for which fill duration (T) scales as the "to-fill" cavity volume over through-inlet flux, i.e., $T \sim$ Volume/area $\times U \sim$ length/U, and up to a non-dimensional parameter K_{engulf}:

$$K_{\text{engulf}} = T_{\text{engulf}} \frac{U_{open}}{L_{\text{body}}}. \tag{3}$$

Equation (3) can also be argued from buccal cavity wall acceleration (Appendix B), as well as from mandible rotation kinematics which yields the predictions shown in Fig. 8.[33] Overall, the idea of a constant non-dimensional engulfment time K_{engulf} appears to make sense for both humpback and blue whales in a lunge-averaged sense.

Variations among the K-values of different whales (same species) are at about 30% for reasons likely due to individual size variation of body features such as VGB and mandible lengths (L_{VGB} and $L_{mandible}$) and skull width (w_{skull}), which are absent in the equation above but present in Eq. (B2) (Appendix B). In the speed data shown in Fig. 7, the value of U_{open} appears largely insensitive to body size—at least for the blue whale data sample shown (e.g., $U_{open} = 3.36$ m/s (SD = 0.33m/s) at 27.4 m body length; and 3.82 m/s (SD = 0.52m/s) at 23.6 m). It would follow that T_{engulf} scales proportionally with body size, thereby determining a good

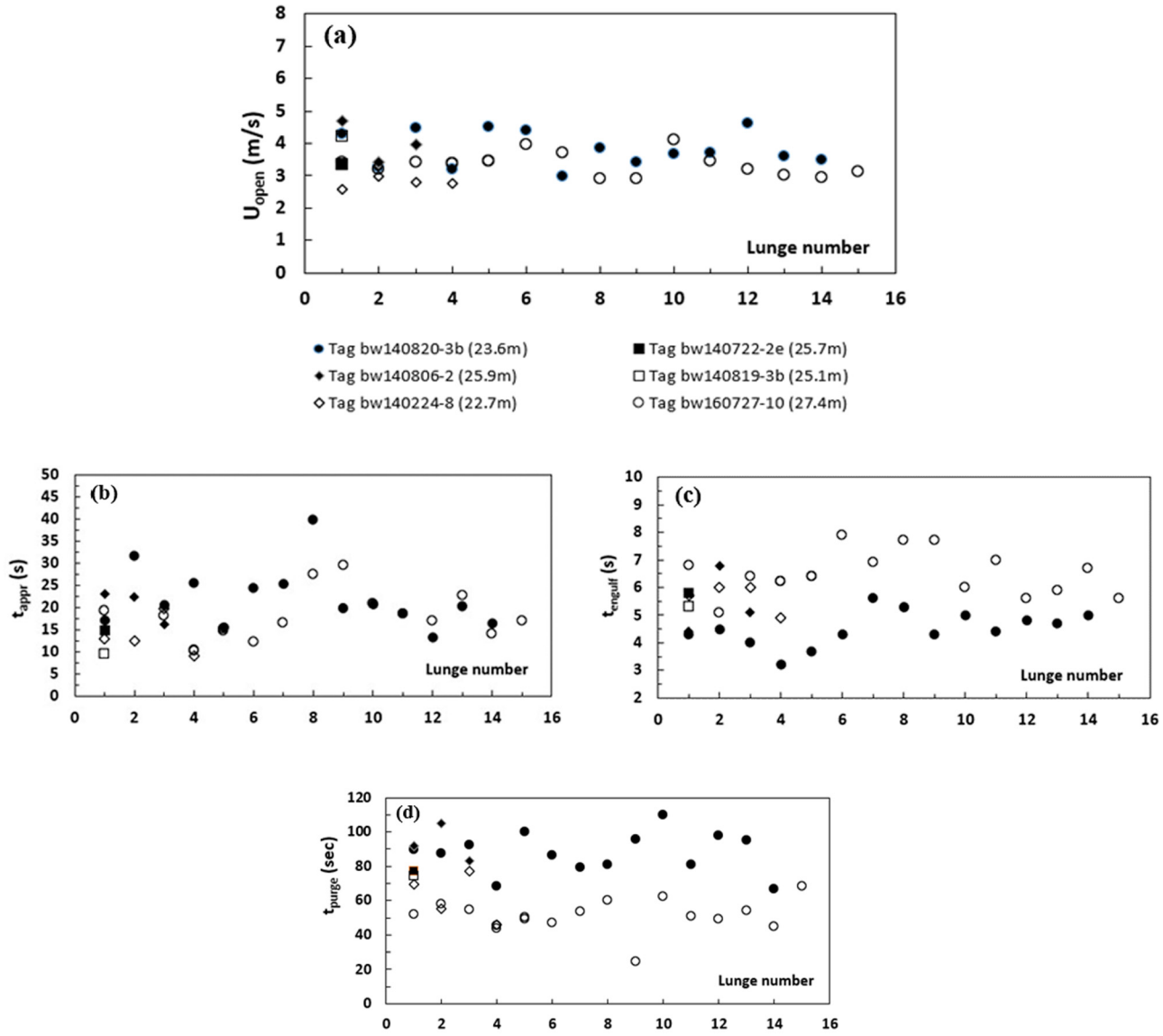

Fig. 7. Bio-logging tag data collected from six blue whales feeding on krill in Monterey Bay, CA, over several lunges and dives (Ref. 17). Swim speed at mouth open (a), followed by the durations of prey approach (b), engulfment (c) and water expulsion-filtration (d). The symbols are described in (a) and correspond to animals of differing body length. The "lunge number" labels the lunges performed over several successive dives by a given animal. For example, and counting about four lunges per dive in blue whales (Ref. 9), the data for the 27 m individual (open circles) would characterize sixteen lunges carried out over four consecutive dives (Fig. 5).

part of the force scaling obtained from Eqs. (2) and (6) (below).

IV. RESULTS—FORCES

A. Coasting engulfment as a perfectly inelastic collision

Omitting the contribution of shape drag permits approximating coasting engulfment as a perfectly inelastic collision. Applying momentum conservation yields $M_{body}\ U_{open} = (M_{body} + M_{water}) \cdot U_{close}$ and solving for U_{close} results in

$$\frac{U_{\text{close}}}{U_{\text{open}}} = \left(\frac{M_{body}}{M_{body} + M_{\text{water}}}\right), \tag{4}$$

a useful formula for the scaling study below. Parameter M_{water} is calculated for maximal engulfment which occurs when the mandibles are lowered to the largest angles possible (≈78°) (Fig. 2),[36] and by approximating the filled buccal cavity as two juxtaposed quarter-ellipsoid sections spanning the skull's width (w_{skull}), mandible length ($L_{mandible}$), and VGB length (L_{VGB})[9–11,22]

$$M_{\text{water}} = \rho_{water} \cdot V_{\text{ventral pouch}} = \rho_{water} \cdot \Psi \left[\frac{\pi}{3} L_{\text{VGB}} L_{\text{mandible}} \frac{1}{2} w_{\text{skull}}\right]. \tag{5}$$

The factor in brackets corresponds to the cavity volume modeled by the ellipsoids,[22] and parameter Ψ, a species-dependent adjustment factor corresponding to the departure from the pure ellipsoid, as caused by mandible dislocation during engulfment.[33] Herein Ψ = 1.17 sin (78°) (blue whale) and = 1.03 sin (78°) (humpback).[9,11] Using the body dimensions listed in Table I (below), ratio $M_{body}/(M_{water}+M_{body})$ ends up varying between 0.6 (L_{body} = 8 m; humpback) and

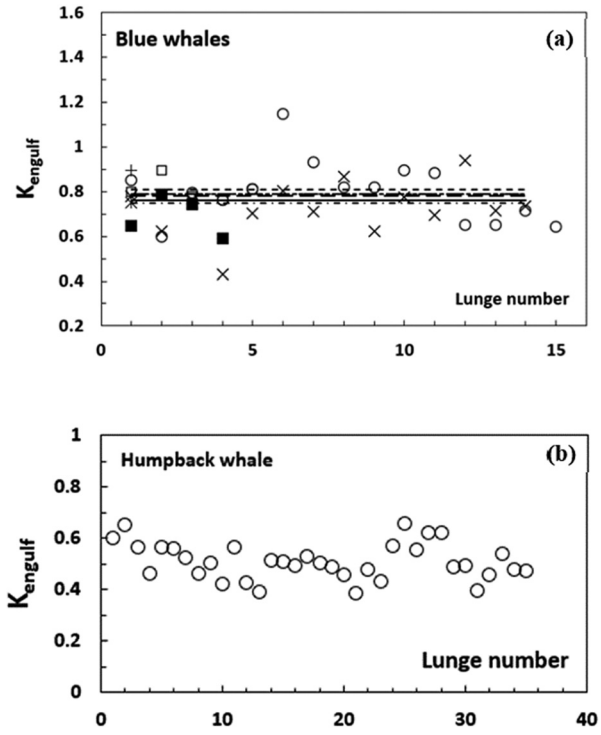

Fig. 8. Non-dimensional engulfment durations (Eq. (3)) constructed from the data of Fig. 7 (Ref. 17). The flat lines correspond to predictions made four years prior to measurement (Ref. 33). For the blue whales of frame (a) tag # bw140820-3b (23.6 m body length; "times" and continuous line); bw140224-8 (22.7 m; filled square and dotted-short-dashed); bw140818-3b (25.1 m; "plus" and dashed-dotted-dotted); bw140722-2e (25.7 m; starburst and dotted-dotted); bw140806-2 (25.9 m; open squares and long dashed); bw160727-10 (27.4 m; open circles and short dashed,). For the humpback whale of frame (b) tag # mn160727-11 (8 m; circles) The "lunge number" label is the same as in Fig. 7.

0.4 (27 m; blue), implying forward speeds at mouth closure reduced to 60% and 40% of the initial speed (U_{open}), respectively.

Interestingly, both left- (LHS) and right-hand (RHS) sides of Eq. (4) can be checked independently given the known scaling of rorqual morphology,[21] the recent capability of measuring body length directly via overflying drones,[37] and the kinematic data collected by bio-logging tags. Averaging over all speed profiles ($U(t)$ vs t) of the lunges carried out by individual blue whales in Cade *et al.* yields $U_{close}/U_{open} \approx 0.43$;[17] and using the likely values of the body morphology applying to similarly-sized whales (Table I), one obtains $M_{body}/(M_{body}+M_{water}) \approx 0.41$, i.e., a near agreement but with errors in the RHS difficult to assess given the uncertainties connected with body mass (see Table I), and also with body length estimates carried out in the absence of drones. (A preliminary analysis of recently-collected tag and drone data suggests LHS/RHS-ratios of 0.92 (SD = 0.10) in blue whale (20 individuals and 660 lunges), and 1.03 (SD = 0.17) in humpback whales (8 and 268) (W. T. Gough, personal communication).)

B. Engulfment drag

Viewing engulfment drag as the reaction to the direct-contact action of the VGB against the water-prey mixture (Fig. 6) allows the calculation here of its time-average $\langle F_D{}^{engulf} \rangle$ in similarity to Eq. (3), while using the equation of motion of the engulfed mass for which the force of the VGB is assumed as dominant. Starting from a state of zero-mass and zero-speed, and ending at mouth-closure time T_{engulf} with a mass M_{water} and at a final speed equal to that of the whale ($U_{water} = U_{whale}(t = T_{engulf}) = U_{close}$) (Fig. 2), one obtains (Appendix C)

$$F_D{}^{engulf} = \left\langle \frac{d}{dt}\left(M_{water}(t)U_{water}(t)\right)\right\rangle = \frac{\left(M_{water}U_{whale}\right)|_{@T_{\text{engulf}}}}{T_{\text{engulf}}}. \tag{6}$$

Using Eq. (6) along with Eqs. (4) and (5) and the tag and body morphology data of Table I yields averaged forces in the range of 19 kN–36 kN in blue whales. Interestingly, these are similar to those of the time-averaged total drag calculated via Eq. (2), thereby pointing to small contributions of shape drag.[11] (Estimates from the recently-collected tag data mentioned above put the ratio $\langle F_D{}^{\text{shape}} \rangle / \langle F_D{}^{\text{engulf}} + F_D{}^{\text{shape}} \rangle$ at 0.14 (SD = 0.15) in blue whales and −0.13 (SD = 0.42) in humpback whales, while showing no intra-species trend versus (adult) body lengths (W. T. Gough, personal communication).)

Being of a pulsed type similar to inflating parachute drag,[38] the peak value of the engulfment force $F_D{}^{engulf}|_{max}$ can also be estimated via the momentum-impulse theorem, which connects the whale's body momentum loss to the impulse of the total (drag) force acting on it ($\Delta P_{if} = \int_i^f F_{total}(t)dt$).[38] Rescaling the integral in terms of engulfment duration and maximum total force sustained yields $M_{whale}[U_{open} - U_{close}] = F_{total}{}^{\max} T_{engulf} I \sim F_D{}^{engulf}|_{\max} T_{engulf} I$, or after solving for maximal engulfment drag

$$F_D{}^{engulf}|_{\max} = M_{body}\left(\frac{U_{\text{open}} - U_{\text{close}}}{I \cdot T_{\text{engulf}}}\right). \tag{7}$$

Parameter I is the result of integral $\int_{open}^{close} F_{total}\ (t)dt / (F_{\text{total}}^{\max} T_{\text{engulf}}) \sim \int_{open}^{close} F_D^{engulf}(t)dt / \left(F_D^{\text{engulf}}|_{\max} T_{engulf}\right)$, with the last step again assuming engulfment drag as the dominant force.[11] Integral I is a non-dimensional measure of the shape of the force vs time curve where, for example, I = 1 when F is constant throughout; I ≈ $\frac{1}{2}$, if shaped like a triangle; or I ≈ 3/8 in the case of engulfment (Appendix D). Actual values of I do reflect the temporal metering of the muscle-based force of the VGB, but it should be remembered that this is an integrated quantity. Typical values of the maximal engulfment drag are shown in Table I, varying between 25 kN and 100 kN, values which are at least twice as large as the time-averaged values. These are also similar to the time-dependent and parametric forces calculated by Potvin *et al.*[11]

C. Engulfment drag vs closed mouth drag

Results of calculations of the various forces at play are shown in Table I, based on the equations above, kinematics from bio-logging tag data,[17] and morphology.[21] Generally, the results proportional to M_{body} are significantly uncertain since obtaining body mass from stranding events and industrialized whaling involves weighing cut-out body parts while trying to limit significant losses of tissue and fluid in the process. On the other hand, those proportional to the engulfed mass M_{water} have smaller uncertainties, being based (via Eq. (5)) on the skull width and lengths of the VGB and

mandibles, all of which are measured accurately-enough. In all cases, the variance includes not only measurement uncertainties, but also more crucially, natural variations among individuals of same body length (and species).[21]

Basic comparisons of the drag generated while the mouth is open (Eqs. (2), (6), and (7)) versus closed (Eqs. (1) and (A1)–(A3)) yield the following results. In the case of a 27 m-long blue whale swimming closed-mouth at a speed of 3.25 m/s, and within a factor-2 uncertainty on the value of the tail heaving drag factor ($\tilde{F}$; Appendix A),[29,30] the corresponding drag turns out at 3740 N, a small value in comparison to the 37,590 N of engulfment drag sustained (±13,420 N; Table I) while decelerating from U_{open} = 3.25 m/s to U_{close} = 1.33 m/s (Fig. 3).[11,17] On the other hand, and with the same mass and speed, maximal engulfment drag ends up at F_{drag}^{enulf} = 100,365 N (±35,127 N; Table I), a value roughly 27 times the closed-mouth drag.

V. DISCUSSION—ALLOMETRIC SCALING AND DYNAMICAL IMPLICATIONS

A. Engulfment capacity

Rorqual whale feeding energetics and dynamics have become part of a wider study of the relationships between body size and filter-feeding in aquatic organisms.[7,39–42] Why this is so rests in good measure with how morphology has coupled with dynamics to exploit prey in manners to insure survival, and for the rorquals, how the coupling has favored large body size. This is modeled here via Eqs. (2) and (6), used along with the known scaling of the morphology[21] duration and speed (Sec. III), and applied to the blue and fin whales—two closely related species of similar shape and size.[21]

The calculations first depend on the morphology of the buccal cavity, here assessed with the quotient M_{water}/M_{body} of the engulfed mass (Eq. (5)) over body mass shown in Fig. 9.[9] The ratio generally increases with size, i.e., starting at $M_{water}/M_{body} \approx 0.6$ where $L_{body} = 10$ m.[21] This trend tracks similarly in the smaller rorqual species, namely, with $M_{water}/M_{body} \approx 1.1$–1.2 in Bryde's whales (*Balaenoptera brydei*) ($L_{body} = 15$ m) and ≈0.45–0.50 in minke whales (*B. acutorostrata*) ($L_{body} = 8$ m).[21] The figure suggests the ratio scaling as $\sim L_{body}^{0.92}$ (fin whales) and $\sim L_{body}^{0.35}$ (blue), with "∼" signifying equality up to a constant factor, rather than remaining insensitive to size as expected from *isometric* scaling where volumes scale as $\sim L_{body}^{3}$ and ratios of volumes as $\sim L_{body}^{0}$ (Table II). Departure from isometry, or *allometry*, occurs in all rorqual species, a result of the skull becoming disproportionally longer and wider during growth into adulthood, leading to scaling laws of the type $L \sim L_{body}^{\alpha}$ ($\alpha > 1$) (Table II).[21,22] Clearly, such allometric scaling is an adaptation that insures larger engulfed volumes and greater harvests of prey to support the metabolic needs of ever-increasing body sizes.[22] Such gain comes with the added bonus of reduced speeds imparted to the engulfed mass at the largest scale, namely, $U_{close}/U_{open} \approx 0.40 \pm 0.03$ (Fig. 9(b) and Table I), in contrast to the smaller rorquals where $U_{close}/U_{open} = M_{body}/M_{body}+M_{water} \approx 0.54$ (Bryde's) and 0.64 (minke). Also interesting is the capping of the momentum transferred to the captured prey-water mixture (Fig. 9(c)), revealing the added benefit of body gigantism as a limiting effect on lost body momentum (and kinetic energy), and ultimately, on the body forces at play (Sec. V).

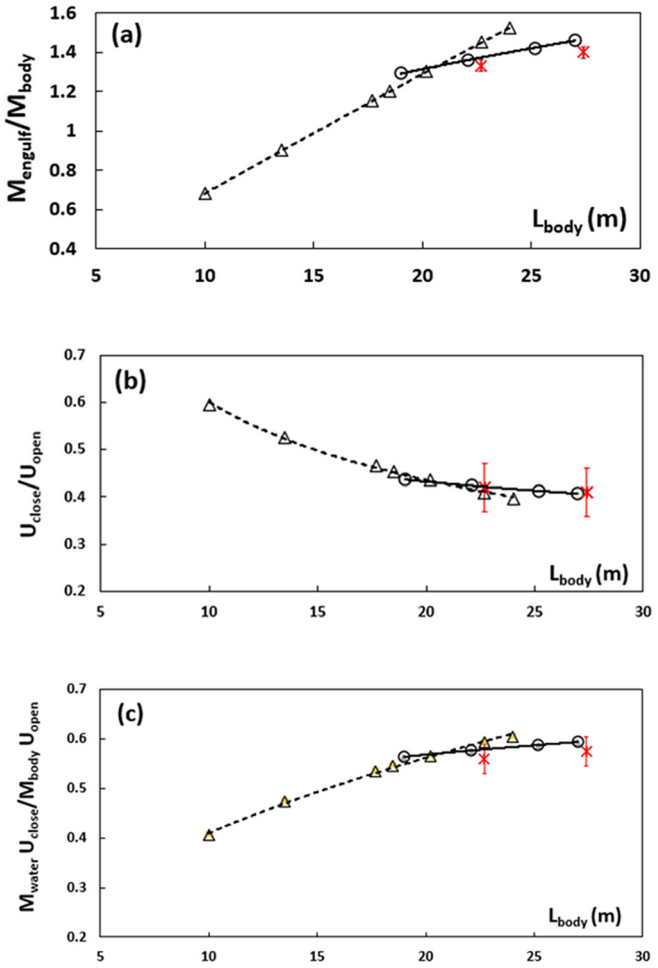

Fig. 9. (a) Engulfed-to-body mass ratio versus body length. Calculated from skull morphological data (Refs. 9 and 21) and Eq. (5), for fin (triangles) and blue whales (circles). Power law fits through these data yields $M_{water}/M_{body} \sim L_{body}^{0.92}$ (fin whales; dashed line) and $\sim L_{body}^{0.35}$ (blue whales; continuous line). (b) Scaling of the velocity ratio U_{close}/U_{open} (Eq. (4)). Power law fits through these data yields $U_{close}/U_{open} \sim L_{body}^{-0.46}$ (fin whales) and $\sim L_{body}^{-0.20}$ (blue whales). (c) Ratio of the momentum gained by the engulfed water (at mouth closure) over initial body momentum (at mouth open); $\sim L_{body}^{-0.45}$ (fin whales) and $\sim L_{body}^{-0.15}$ (blue whales). Uncertainties on the scaling curves are similar to the standard deviations shown in Table I (starburst).

B. Engulfment force exerted by the body

The scaling of the average engulfment force (Eq. (6)) follows from the scaling laws on engulfment time (Eq. (3)) and swim speed at mouth-opening (U_{open}). Apart from the data of Cade *et al.*[17] collected from small populations of humpback and blue whales, the scaling law for U_{open} isn't well

Table II. Scaling exponents with respect to body length L_{body}, of a given observable ($Z \sim L_{body}^{\beta}$); obtained from averaging over intra-specific individual variations (Refs. 9 and 21).

Z	Humpback β	Fin β	Blue β	Isometric scaling
M_{body}	4.17	2.74	3.54	3
L_{VGB}	1.19	1.16	1.19	1
L_{jaw}	1.21	1.29	1.47	1
W_{head}	1.04	1.21	1.20	1
M_{water}	3.44	3.66	3.86	3

known. Provisionally using the size-independence suggested in Fig. 7 for blue whales ($U_{open} \sim L_{body}{}^{0}$), one arrives at $T_{engulf} \sim L_{body}$ and ultimately to the forces $\langle F_{engulf} \rangle$ scaling as $L_{body}{}^{2.20}$ (fin whale) and $\sim L_{body}{}^{2.69}$ (blue) as shown in Fig. 10(a). Similar trends apply to the maximal engulfment force (Eq. (7)) and fluking thrust (see Eq. (1), after neglecting shape drag). Figure 10(a) shows that these results are also insensitive to the scaling of the mouth-open speed, as demonstrated with the use of an alternative scaling law, e.g., $U_{open} = 0.15\ L_{body}$, constructed for correlating data collected a decade ago on humpback, fin, and blue whales.[9] Clearly, body mass drives the magnitude of the force, i.e., over that of the acceleration scale U_{open}/T_{engulf}.

Altogether different scaling trends arise when considering the body force generated by per kilograms of mass ($\langle F_D{}^{engulf} \rangle / M_{body}$). Equations (5) and (6), and the duration and speed scaling laws used in Fig. 8, lead to the results shown in Fig. 10(b) in the case of the two mouth-open speed scaling scenarios discussed above. Where $U_{open} \sim L_{body}{}^{0}$, the specific force decreases with size, in agreement (within uncertainties) with the tagged individuals showcased in Table I: namely, $\langle F_D{}^{engulf} \rangle / M \approx 0.3$N/kg for both 23 and 27 m blue whales (Fig. 10(b)), and 1.1 N/kg for the 8 m humpback whale which, incidentally, approached prey at speeds similar to the blue whales' (3.8 m/s, vs 2.8 m/s and 3.2 m/s). Here, and according to Eqs. (6) and (C2), the scaling of the specific force ultimately rests on the scaling of the ratio U_{open}/T_{engulf}, as (likely) determined from the whales' behaviors during prey approach and engulfment.

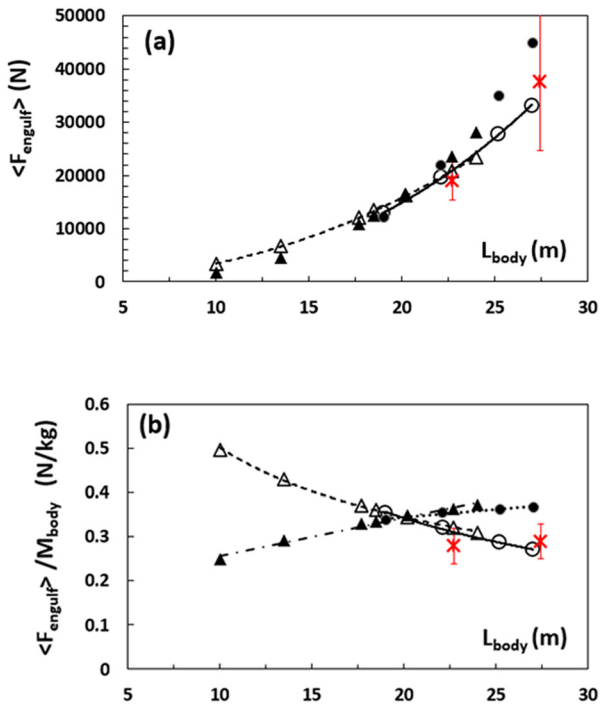

Fig. 10. Time-averaged coasting engulfment drag and mass-specific engulfment drag versus body length for fin (triangles) and blue (circles) whales. In both frames, the open symbols correspond to the calculated values from Eq. (6), skull morphological data (Refs. 9 and 21), and $U_{open} = 3$ m/s at all L_{body}; and closed symbols, to $U_{open} = 0.15\ L_{body}$. In (a), the lines follow power law fits for which $\langle F_{engulf} \rangle \sim 21.9\ L_{body}{}^{2.20}$ (fin whale; dashed line) and $\sim 4.73\ L_{body}{}^{2.69}$ (blue whale; continuous). In (b) and for the fin whales, the curves are fitted to $\langle F \rangle / M \sim 1.75\ L_{body}{}^{-0.54}$ (dashed) and $\sim 0.1708 + 0.0087\ L_{body}$ (dotted-dashed); for the blue whales, to $\langle F \rangle / M \sim 3.46\ L_{body}{}^{-0.771}$ (continuous) and $\sim 0.2742 + 0.0035\ L_{body}$ (dots). Uncertainties on the scaling curves are similar to the standard deviations shown in Table I (starburst).

Although detailed studies of VGB muscle action are still in the future,[12,13] visuals of buccal cavity expansion generally suggest muscle generating tension during elongation (a.k.a., "eccentric pulls").[12] At muscle fiber-level, eccentric tension isn't as sensitive to the elongation rate as for fast contractions which generate significantly less force.[43] With engulfment drag arising as a reaction to the (longitudinal) pushing action of the VGB onto the engulfed mass, one is left with the latter metering force in proportion to total muscle mass rather than through elongation rate. This, in turns, would lead to the hypothesis in which a smaller specific force arises from the use of smaller proportions of muscle, at least to effect foraging. In other words, the coasting engulfment mechanism described here would make prey collection more efficient in terms of the required body forces and at the largest scale, that is, as long as both larger and smaller individuals of a species approach prey at similar speeds.

VI. CONCLUDING REMARKS

This paper has shown how coasting engulfment, together with the allometry of the buccal cavity, approach speeds and engulfment duration, combine in ways that favor large body size among the largest rorquals. Whether the scaling of the specific force among the smaller rorquals follows the trend hinted at in Fig. 10 isn't known. Recently collected kinematic data on minke and Bryde's whales (9–14 m) have yet to be fully analyzed and published. Such data are eagerly awaited for further testing of the coasting engulfment paradigm, as well as for uncovering the scaling laws of important ratios such as U_{open}/T_{engulf} and U_{close}/U_{open} which, in the end, drive the scaling of the specific engulfment force.

Smaller rorquals such as the minke, Bryde's, and humpback whales have also been observed fluking while engulfing schools of forage fish, but at significantly slower speeds (<2 m/s) (Fig. 3).[17,18] Clearly, fluking in a high-drag (mouth-open) configuration requires more effort as suggested by the net forces involved when accelerating at speed increments similar in absolute value to those of coasting blue whales (Fig. 3)

$$\left\langle F_{thrust} - F_{drag}{}^{\text{powered engulf}} \right\rangle = \frac{M_{body}(U_{close} - U_{start})}{T_{\text{engulf}}} \sim \left\langle |F_{drag}{}^{\text{coasting engulf}}| \right\rangle. \tag{8}$$

Thus with average accelerations generated at $U_{close} = 3.5$ m/s, $U_{open} = 1.5$ m/s, and $T_{engulf} = 6$ s, Eq. (8) yields average thrust forces amounting to about twice the drag (and VGB active push), thereby tripling the net body-supplied force (i.e., of the VGB and fluking tail muscle). On the other hand, and as further explored in a sequel paper, the required body forces and energies generated at low speed (<2 m/s) turn out similar to those of coasting engulfment carried out at those same speeds. Whether powered engulfment also yields a dynamical efficiency at large body size remains a question to be further investigated.

Other dynamical aspects favoring large rorquals can be revealed by looking at Life's energy angle.[7,18] It is known already that mass-specific metabolic expenditures during resting decrease at large body size, i.e., roughly as $\sim 1/L_{body}{}^{0.25}$ for land vertebrates[44] and $\sim 1/L_{body}{}^{0.32}$ in cetaceans.[45] However,

and during foraging, prey abundance and energy contents become key factors driving the energetic efficiency of feeding, and not surprisingly, the gigantism displayed by both large toothed and edentulous cetaceans.[7,46] But, as will be discussed in future work, the energetic efficiency of coasting engulfment is also driven by dynamics, enhanced even, for example when the prey-approach speeds are near the minimum required for coasting over an entire mouth open-closure cycle.

ACKNOWLEDGMENTS

J.A.G. and D.E.C. were supported in part by grants from the National Science Foundation (NSF) (IOS-1656676), the Office of Naval Research (N000141612477), and a Terman Fellowship from Stanford University; and J.P. by a grant from the NSF (IOS-1656656). The authors thank F. E. Fish, J. H. Kennedy, N. E. Pyenson, and P. Segre for stimulating discussions. They are also grateful to D. J. Albert and A. Boersma for the use of their artwork, and to W. T. Gough for communicating preliminary results from his bio-logging tag data analysis.

APPENDIX A: CLOSED-MOUTH DRAG (DURING PREY-APPROACH)

Drag for highly streamlined objects is estimated from an expression originally devised for airships,[47] and later applied to cetaceans[48,49] after insertion of a correction factor ($\tilde{F}(U)$) accounting for the heaving of the tail and head during active swimming[49]

$$F_{\text{drag}}^{\text{parasite}} = \frac{1}{2}\rho_w S_{\text{wet}} C_D(t) U(t)^2 \equiv \Gamma U(t)^{1.8}, \tag{A1}$$

$$C_D(t) = \tilde{F}\left[\frac{0.072}{\left(L_{body}U(t)/\nu\right)^{1/5}}\right] \cdot \left[1 + 1.5\left(\frac{w_{\max}}{L_{\text{body}}}\right)^{\frac{3}{2}} + 7.0\left(\frac{w_{\max}}{L_{\text{body}}}\right)^{3}\right]. \tag{A2}$$

Parameters S_{wet}, U, and ρ_w correspond to the wetted body surface area, the whale's swimming speed, and sea water density (1025 kg/m^3), respectively. In cetaceans, one uses $S_{wet} = 0.08\, m^2/kg^{0.65}\ (M_{body}{}^{0.65})$.[49,50] C_D is the drag coefficient arising from the viscous friction between the body and its boundary layer (first bracket), and the pressure gradient caused by near-wake turbulence (second bracket).[47,51] In the latter L_{body} and w_{max} correspond to the body length and maximum width, respectively. The ratio $U(t)L_{body}/\nu$ is the Reynolds number with ν as the water kinematic viscosity (1.19×10^{-6} m^2/s). The first bracket in Eq. (A2) applies because the whales' large size, swim speed, ratio L_{body}/w_{max}, and Reynolds number (12–27 m, 1–3 m/s, 5–10, and $>10^6$, respectively) all contribute to the suppression of pressure gradients and attendant flow separation over the body surface.[51,52] Finally, and with respect to coefficient $\tilde{F}$, comparison with direct calculation of the thrust by idealized rigid lunate tails suggests $\tilde{F} \sim 1$–3 at $Re \sim 10^7$, hence the value $\tilde{F} \sim 2.0$ used herein.[49] Note that Eq. (A2) omits a surface wave drag correction,[49] as most of the lunges described here are performed away from the surface (Fig. 5).

To the drag of Eq. (A1), usually valid at constant-speeds, one adds the contribution of the so-called "acceleration reaction" (or "added mass") whenever a whale is accelerating (a)[52,53]

$$F_{drag}^{ar} = k_{added}\rho_{water}V_{body}a = k_{added}M_{body}a. \tag{A3}$$

V_{body} is the whale's body volume, and the last step in Eq. (A3) is based on approximating a whale's body density with that of seawater. The added mass coefficient k_{added} is calculated from inviscid hydrodynamics.[53,54] As currently unknown in cetaceans, it is approximated by coefficients associated with prolate ellipsoids of revolution, namely, $k_{added} = 0.059$, 0.045, 0.036, and 0.029 for $w_{max}/L_{body} \sim 5$, 6, 7, and 8 typical of rorqual body aspect ratios.[52,53] Along with the VGB-generated engulfment drag, the acceleration reaction is an inertial source of drag which appears even in the absence of viscosity. It arises from the need to increase, over time, the kinetic energy of the fluid near an accelerating body,[54] as imparted by the forward or rearward shift of the pressure gradient along its surface (in comparison to the steady state pressure profile). The first bracket in Eq. (A2) remains valid in accelerated motions, again due to high body fineness and Reynolds numbers, i.e., conditions which (again) limit the importance of surface pressure gradients from head to tail, and most importantly, suppress boundary layer separation and (large) vortex shedding.[55]

Approximating $U(t)$ as the sum U_{start} + at (with $a = (U_{open} - U_{start})/T_{approach}$), time-averaging the three equations above during prey approach yields the following result, which can be combined with Eq. (1) to get an estimate of the fluking thrust:

$$\left\langle F_{\text{drag}}^{shape} \right\rangle = \frac{\Gamma}{2.8T_{approach}}\left({U_{open}}^{2.8} - {U_{start}}^{2.8}\right) + k_{added}M_{body}\left(\frac{U_{open} - U_{start}}{T_{approach}}\right). \tag{A4}$$

APPENDIX B: INFLATION DURATION SCALING

An expression for the scaling of inflation duration of a bag-like structure, versus inlet fluid speed, can be derived by looking at a cavity as filling with an incompressible fluid of mass density ρ entering with speed U (time-averaged) through a fixed diameter inlet, to expand and impart its walls with an acceleration a_{expand} over a distance scale d and duration $T_{inflate}$ (Fig. 11). Area A characterizes the accelerating sections of the bag walls and, using constant-acceleration kinematics along with zero-initial wall speed, leads to: $d \sim \frac{1}{2}\, a_{expand}\, (T_{inflate})^2$. In cases analogous to common kitchen garbage bags in which wall elasticity is absent, acceleration during expansion is driven by the internal dynamical pressure ($\frac{1}{2}\rho U^2$) and leads to $a_{expand} = A\,(\frac{1}{2}\rho U^2)/m_{wall}$, with m_{wall} corresponding to the mass of the accelerating wall sections. This is a result that describes wall motions controlled solely by internal pressure, rather than by pressure combined with wall elasticity. On the other hand, the hydrodynamic modeling showcased in Fig. 3 is based on VGB muscular contraction forces which are also tuned to dynamic pressure, via a dimensionless "total-force" coefficient k.[11] In this case, the wall acceleration would become: $a_{expand} = A\,(k\,\frac{1}{2}\rho U^2)/m_{wall}$.

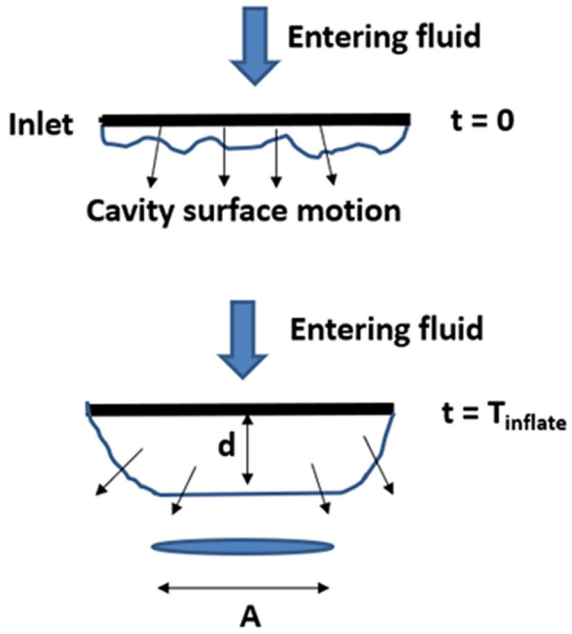

Fig. 11. Schematics of a previously folded "bag" (top) inflating to a final configuration (bottom), in the case of a fixed-diameter inlet.

Merging the latter with constant acceleration kinematics and solving for inflation time will result in

$$T_{\text{inflate}} \sim \frac{1}{U_{open}}\sqrt{\frac{4m_{wall}d}{kA\rho}} \equiv K_{\text{inflate}}\left(\frac{L}{U_{open}}\right), \tag{B1}$$

with the last step added to emphasize the similarity with Eq. (3). Note that the details of a cavity's architecture and size would enter in the square root (including k). With krill feeding whales, Eq. (B1) would apply to the duration of mouth-open-to-maximum-gape, which is basically half of engulfment time,[17,33] leading to $K_{inflate} = \frac{1}{2} K_{engulf}$. Note that incorporating further morphological details would result in the wall being composed of a number of folds called "furrows" (N_{furrow}) adjacent to thick slats of hardened skin linked by pleated soft tissue.[2,14] With a slat width w_{slat} and mass density close to that of sea water (ρ), and with the ratio m_{wall}/A ρ and d approximated as w_{slat} and $w_{head}/2N_{furrow}$, respectively, coefficient $K_{inflate}$ will read as

$$K_{\text{inflate}} = \frac{1}{L}\sqrt{\frac{4m_{wall}d}{kA\rho}} \sim \frac{1}{L}\sqrt{\frac{2w_{slat}w_{head}}{kN_{furrow}}}. \tag{B2}$$

This result hints at $K_{inflate}$ and K_{engulf} scaling as $\sim L^0$ in an isometric world where both w_{furrow} and $L_{mandible}$ are proportional to L; or as up to $K_{expand} \sim L^{1.2}$ in the allometric world of the whales (Table II), leading to the individual-to-individual variations shown in Fig. 8.

APPENDIX C: TIME-AVERAGED ENGULFMENT DRAG

Viewing lunge-feeding as a colliding two-body system permit non-trivial estimations of the time-averaged value of the engulfment drag as follows. Starting with the general definition $\langle F\rangle = 1/T\int_0^T F(t)dt$ in which engulfment drag equal to the rate of momentum change by the engulfed mass over $T = T_{engulf}$, one has $F_{engulf}(t) = \frac{d}{dt}(M_{water}(t)V_{water}(t))$. Assuming $M_{water}(0) = 0$ and $U_{water}(0) = 0$ yields

$$\left\langle {F_{drag}}^{engulf}\right\rangle = \frac{1}{T_{\text{engulf}}}\int_0^{T_{engulf}} \frac{d}{dt}(M_{water}(t)U_{water}(t))dt = \frac{(M_{water}U_{water})|T_{\text{engulf}}}{T_{\text{engulf}}}. \tag{C1}$$

Taking the whale and engulfed mass to be a perfectly inelastic colliding two-body system in which $U_{water} = U_{whale} = U_{close}$ (at T_{engulf}) is given in Eq. (4), the above ends up as

$$\left\langle {F_{drag}}^{engulf}\right\rangle = \frac{M_{water}(T_{\text{engulf}})}{T_{\text{engulf}}}U_{\text{open}} \times \left(\frac{M_{whale}}{M_{whale} + M_{\text{water}}(T_{\text{engulf}})}\right). \tag{C2}$$

APPENDIX D: SHAPE OF ENGULFMENT DRAG VERSUS TIME

Equation (7) involves evaluating parameter I, a non-dimensional measure of the shape of engulfment drag versus time

$$I \equiv \int_{open}^{close}\frac{F_{total}(t)}{F_{\text{total}}^{\max}T_{\text{engulf}}}dt \sim \int_{open}^{close}\frac{F_D^{engulf}(t)}{F_D^{\text{engulf}}|_{\max}T_{engulf}}\text{dt}. \tag{D1}$$

With engulfment drag being a derived construct rather than a datum obtained from tags, integral I is evaluated from the results of more detailed hydrodynamic modeling.[11] An approximate (linear) rendition of it is shown in Fig. 12, in the form of two juxtaposed triangles for which the area-under-the-curve is readily obtained as $\sim {F_D}^{engulfed}|_{max}\ T\ (1/4 + Y/4)$ with $Y \sim \frac{1}{2}$ (Fig. 5 of Ref. 11), leading to $I \sim 3/8$.

[a]Current address: Institute of Marine Science, University of California,

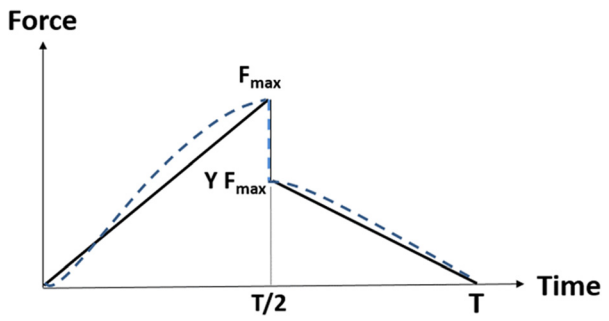

Fig. 12. Schematic rendition of the temporal variation of engulfment drag (dashed line) (Ref. 11), in comparison to the approximate linear form used for the estimation of the curve shape parameter I in Eqs. (7) and (D1) (continuous line).

Santa Cruz, Santa Cruz, California 95060.

[1]M. Denny, *Ecological Mechanics: Principles of Life's Physical Interactions* (Princeton U. P., Princeton, 2015).
[2]J. A. Goldbogen, D. E. Cade, J. Calambokidis, A. S. Friedlaender, J. Potvin, P. S. Segre, and A. J. Werth, "How baleen whales feed: The biomechanics of engulfment and filtration," Annu. Rev. Mar. Sci. **9**, 367–386 (2017).
[3]A. J. Werth, J. Potvin, R. E. Shadwick, M. M. Jensen, D. E. Cade, and J. A. Goldbogen, "Filtration area scaling and evolution in mysticetes: Trophic niche partitioning and the curious cases of sei and pygmy right whales," Biol. J. Linn. Soc. **125**(2), 264–279 (2018).
[4]F. G. Marx, O. Lambert, and M. D. Uhen, *Cetacean Paleobiology* (John Wiley & Sons, New Jersey, 2016).
[5]Pierre-Henry Fontaine, *Whales and Seals: Biology and Ecology* (Schiffer Pub Limited, Pennsylvania, 2007).
[6]Baleen are narrowly spaced, thin triangular plates made of keratinous tissue suspended from the palatal gingiva, numbering at 200–400 on each side of the palate (Fig. 2).
[7]J. A. Goldbogen, D. E. Cade, D. M. Wisniewska, J. Potvin, P. S. Segre, M. S. Savoca, E. L. Hazen, M. F. Czapanskiy, S. R. Kahane-Rapport, S. L. DeRuiter, S. Gero, H. P. Tønnesen, W. I. Gough, M. B. Hanson, M. M. Holt, F. H. Jensen, M. Simon, A. K. Stimpert, P. Arranz, D. W. Johnston, D. P. Nowacek, S. E. Parks, F. Visser, A. S. Friedlaender, P. L. Tyack, P. T. Madsen, and N. D. Pyenson, "Why whales are big but not bigger: Physiological drivers and ecological limits in the age of ocean giants," Science **366**(6471), 1367–1372 (2019).
[8]*Escaping from Predators: An Integrative View of Escape Decisions*, edited by W. E. Cooper, W. E. Cooper, Jr. and D. T. Blumstein (Cambridge U. P., Cambridge, 2015).
[9]J. A. Goldbogen, J. Calambokidis, D. A. Croll, M. F. McKenna, E. Oleson, J. Potvin, N. D. Pyenson, G. Schorr, R. E. Shadwick, and B. R. Tershy, "Scaling of lunge-feeding performance in rorqual whales: Mass-specific energy expenditure increases with body size and progressively limits diving capacity," Funct. Ecol. **26**(1), 216–226 (2012).
[10]J. Potvin, J. A. Goldbogen, and R. E. Shadwick, "Passive versus active engulfment: Verdict from trajectory simulations of lunge-feeding fin whales *Balaenoptera physalus*," J. R. Soc. Interface **6**(40), 1005–1025 (2009).
[11]J. Potvin, J. A. Goldbogen, and R. E. Shadwick, "Metabolic expenditures of lunge feeding rorquals across scale: Implications for the evolution of filter feeding and the limits to maximum body size," PLoS One **7**(9), e44854 (2012).
[12]R. E. Shadwick, J. A. Goldbogen, J. Potvin, N. D. Pyenson, and W. Vogl, "Novel muscle and connective tissue design enables high extensibility and controls engulfment volume in lunge-feeding rorqual whales," J. Exp. Biol. **216**(14), 2691–2701 (2013).
[13]R. E. Shadwick, J. Potvin, and J. A. Goldbogen, "Lunge feeding in rorqual whales," Physiology **34**(6), 409–418 (2019).
[14]A. J. Werth and H. Ito, "Sling, scoop, and squirter: Anatomical features facilitating prey transport, processing, and swallowing in rorqual whales (Mammalia: Balaenopteridae)," Anat. Rec. **300**(11), 2070–2086 (2017).
[15]The VGB consists of the pleated tissue covering the belly-side of the body (Fig. 2), which is kept folded and retracted by muscle and elastic tissue during closed-mouth travel. During engulfment, muscle tension is relaxed to allow distention of the ventral skin, but only partially to prevent the muscle fibers from stretching beyond their breaking point, which is shorter than the allowable displacements of the skin's elastin matrix (as found in dead tissue) (Ref. 12). Muscle use has also been proposed as a means to manage loads on the body (Ref. 10).
[16]D. Wiley, C. Ware, A. Bocconcelli, D. Cholewiak, A. Friedlaender, M. Thompson, and M. Weinrich, "Underwater components of humpback whale bubble-net feeding behaviour," Behaviour **148**(5), 575–602 (2011).
[17]D. E. Cade, A. S. Friedlaender, J. Calambokidis, and J. A. Goldbogen, "Kinematic diversity in rorqual whale feeding mechanisms," Curr. Biol. **26**(19), 2617–2624 (2016).
[18]D. E. Cade, N. Carey, P. Domenici, J. Potvin, and J. A. Goldbogen, "Predator-informed looming stimulus experiments reveal how large filter feeding whales capture highly maneuverable forage fish," Proc. Natl. Acad. Sci. **117**(1), 472–478 (2020).
[19]C. M. Jurasz and V. P. Jurasz, "Feeding modes of the humpback whale (*Megaptera Novaeangliae*) in southeast Alaska," Sci. Reporting Whales Res. Inst. **31**, 69–83 (1979).
[20]M. Simon, M. Johnson, and P. T. Madsen, "Keeping momentum with a mouthful of water: Behavior and kinematics of humpback whale lunge feeding," J. Exp. Biol. **215**(21), 3786–3798 (2012).
[21]S. R. Kahane-Rapport and J. A. Goldbogen, "Allometric scaling of morphology and engulfment capacity in rorqual whales," J. Morphol. **279**(9), 1256–1268 (2018).
[22]J. A. Goldbogen, J. Potvin, and R. E. Shadwick, "Skull and buccal cavity allometry increase mass-specific engulfment capacity in fin whales," Proc. R. Soc. B: Biol. Sci. **277**(1683), 861–868 (2009).
[23]Mark P. Johnson and Peter L. Tyack, "A digital acoustic recording tag for measuring the response of wild marine mammals to sound," IEEE J. Oceanic Eng. **28**(1), 3–12 (2003).
[24]P. Miller, T. Narazaki, S. Isojunno, K. Aoki, S. Smout, and K. Sato, "Body density and diving gas volume of the northern bottlenose whale (Hyperoodon ampullatus)," J. Exp. Biol. **219**, 2458–2468 (2016).
[25]L. N. Cooper, N. Sedano, S. Johansson, B. May, J. D. Brown, C. M. Holliday, B. W. Kot, and F. E. Fish, "Hydrodynamic performance of the minke whale (Balaenoptera acutorostrata) flipper," J. Exp. Biol. **211**(12), 1859–1867 (2008).
[26]P. S. Segre, D. E. Cade, F. E. Fish, J. Potvin, A. N. Allen, J. Calambokidis, A. S. Friedlaender, and J. A. Goldbogen, "Hydrodynamic properties of fin whale flippers predict maximum rolling performance," J. Exp. Biol. **219**(21), 3315–3320 (2016).
[27]P. S. Segre, D. E. Cade, J. Calambokidis, F. E. Fish, A. S. Friedlaender, J. Potvin, and J. A. Goldbogen, "Body flexibility enhances maneuverability in the world's largest predator," Integr. Comp. Biol. **59**(1), 48–60 (2019).
[28]A. C. Gleiss, J. Potvin, J. J. Keleher, J. M. Whitty, D. L. Morgan, and J. A. Goldbogen, "Mechanical challenges to freshwater residency in sharks and rays," J. Exp. Biol. **218**(7), 1099–1110 (2015).
[29]F. E. Fish and J. J. Rohr, "Review of dolphin hydrodynamics and swimming performance," Report No. SPAWAR/CA-TR-1801, Space and Naval Warfare Systems Command, San Diego, CA (1999).
[30]Frank E. Fish *et al*., "Measurement of hydrodynamic force generation by swimming dolphins using bubble DPIV," J. Exp. Biol. **217**(2), 252–260 (2014).
[31]Longitudinally, such work arises from the differing displacements by the whale and mixture as a consequence of deformation in the direction of motion.
[32]N. D. Pyenson, J. A. Goldbogen, A. W. Vogl, G. Szathmary, R. L. Drake, and R. E. Shadwick, "Discovery of a sensory organ that coordinates lunge feeding in rorqual whales," Nature **485**(7399), 498–500 (2012).
[33]J. Potvin, J. A. Goldbogen, and R. E. Shadwick, "Scaling of lunge feeding in rorqual whales: An integrated model of engulfment duration," J. Theor. Biol. **267**(3), 437–453 (2010).
[34]D. E. Cade, K. R. Barr, J. Calambokidis, A. S. Friedlaender, and J. A. Goldbogen, "Determining forward speed from accelerometer jiggle in aquatic environments," J. Exp. Biol. **221**(2), jeb170449 (2018).
[35]W. M. Hamner and P. P. Hamner, "Behavior of Antarctic krill (*Euphausia superba*): Schooling, foraging, and antipredatory behavior," Can. J. Fish. Aquat. Sci. **57**(S3), 192–202 (2000).
[36]J. A. Goldbogen, N. D. Pyenson, and R. E. Shadwick, "Big gulps require high drag for fin whale lunge feeding," Mar. Ecol. Prog. Ser. **349**, 289–301 (2007).
[37]F. Christiansen, M. Sironi, M. J. Moore, M. Di Martino, M. Ricciardi, H. A. Warick, D. J. Irschick, R. Gutierrez, and M. M. Uhart, "Estimating body mass of free-living whales using aerial photogrammetry and 3D volumetrics," Methods Ecol. Evol. **10**(12), 2034–2044 (2019).
[38]J. Potvin, "Universality considerations for graphing parachute opening shock factor versus mass ratio," J. Aircr. **44**(2), 528–538 (2007).
[39]M. Friedman, K. Shimada, L. D. Martin, M. J. Everhart, J. Liston, A. Maltese, and M. Triebold, "100-million-year dynasty of giant planktivorous bony fishes in the Mesozoic seas," Science **327**(5968), 990–993 (2010).
[40]J. A. Goldbogen and P. T. Madsen, "The evolution of foraging capacity and gigantism in cetaceans," J. Exp. Biol. **221**(11), jeb166033 (2018).
[41]N. Carey and J. A. Goldbogen, "Kinematics of ram filter feeding and beat-glide swimming in the northern anchovy Engraulis mordax," J. Exp. Biol. **220**(15), 2717–2725 (2017).
[42]R. McNeill Alexander, "All-time giants: the largest animals and their problems," Palaeontology **41**(6), 1231–1246 (1998).
[43]R. M. Alexander, *Principles of Animal Locomotion* (Princeton U. P., Princeton, NJ, 2003).

[44]M. Kleiber, *The Fire of Life: An Introduction to Animal Energetics* (Robert E. Kreiger Co, Huntington, New York, 1975).
[45]T. M. Williams and J. L. Maresh, "Exercise energetics," In *Marine Mammal Physiology: Requisites for Ocean Living*, edited by M. A. Castellini and J. A. Mellish (CRC Press, Florida, 2015).
[46]T. M. Williams, "The biology of big," Science **366**(6471), 1316–1317 (2019).
[47]R. D. Blevins, *Applied Fluid Dynamics Handbook* (Van Nostrand Reinhold Co., New York, NY, 1984), p. 568.
[48]G. L. Kooyman, *Diverse Divers: Physiology and Behavior* (Springer Science & Business Media, Berlin, 2012), Vol. 23.
[49]F. E. Fish, "Comparative kinematics and hydrodynamics of odontocete cetaceans: Morphological and ecological correlates with swimming performance," J. Exp. Biol. **201**(20), 2867–2877 (1998).
[50]B. L. Woodward, J. P. Winn, and F. E. Fish, "Morphological specializations of baleen whales associated with hydrodynamic performance and ecological niche," J. Morphol. **267**(11), 1284–1294 (2006).
[51]J. A. Goldbogen, F. E. Fish, and J. Potvin, "Hydrodynamics," In *Marine Mammal Physiology: Requisites for Ocean Living*, edited by M. A. Castellini and J. A. Mellish (CRC Press, Florida, 2015).
[52]A. C. Gleiss, J. Potvin, and J. A. Goldbogen, "Physical trade-offs shape the evolution of buoyancy control in sharks," Proc. R. Soc. B: Biol. Sci. **284**(1866), 1345–1355 (2017).
[53]H. Lamb, *Hydrodynamics*, 6th ed. (Cambridge U. P., Cambridge, 1932).
[54]J. N. Newman, *Marine Hydrodynamics* (Massachusetts Institute of Technology, Cambridge, Massachusetts, 1977).
[55]T. Sarpkaya, *Wave Forces on Offshore Structures* (Cambridge U. P., Cambridge, 2010).

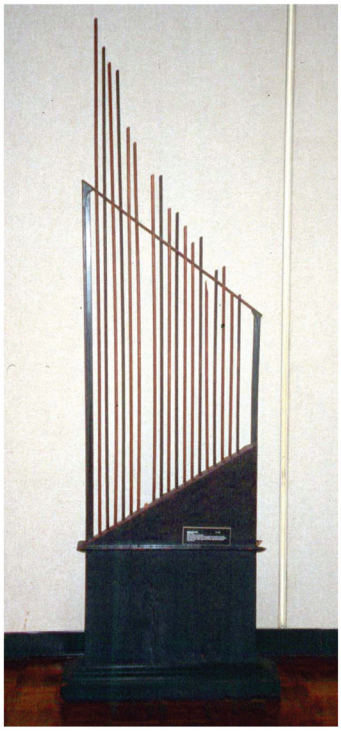

Marloye's Harp

Marloye was a Parisian maker of acoustical apparatus in the middle years of the nineteenth century, and is best known for his technique of mounting tuning forks on boxes cut to half or quarter wavelengths. In the following article I discussed the sounds produced when a rod is stroked and sent into longitudinal oscillations (Marloye's harp) and when it is set into transverse oscillations (the Thumb Piano): Thomas B. Greenslade, Jr., "Marloye's Harp and the Thumb Piano", *Phys. Teach.*, 38, 310-312 (2001). The apparatus is on display at the museum of the University of Mississippi. (Picture and text by Thomas B. Greenslade, Jr., Kenyon College)